Ultrasound in Med. & Biol., Vol. 43, No. 12, pp. 2848–2861, 2017

0301-5629/$ - see front matter

https://doi.org/10.1016/j.ultrasmedbio.2017.08.938

● *Original Contribution*

NUMERICAL AND EXPERIMENTAL STUDY OF MECHANISMS INVOLVED IN BOILING HISTOTRIPSY

Ki Joo Pahk,*[1] Pierre Gélat,* David Sinden,[†] Dipok Kumar Dhar,[‡] and Nader Saffari*

* Department of Mechanical Engineering, University College London, London, UK; [†] Acoustics Group, National Physical Laboratory, Teddington, UK; and [‡] Institute for Liver and Digestive Health, Royal Free Hospital, University College London, London, UK

(*Received* 21 *February* 2017; *revised* 16 *August* 2017; *in final form* 17 *August* 2017)

Abstract—The aim of boiling histotripsy is to mechanically fractionate tissue as an alternative to thermal ablation for therapeutic applications. In general, the shape of a lesion produced by boiling histotripsy is tadpole like, consisting of a head and a tail. Although many studies have demonstrated the efficacy of boiling histotripsy for fractionating solid tumors, the exact mechanisms underpinning this phenomenon are not yet well understood, particularly the interaction of a boiling vapor bubble with incoming incident shockwaves. To investigate the mechanisms involved in boiling histotripsy, a high-speed camera with a passive cavitation detection system was used to observe the dynamics of bubbles produced in optically transparent tissue-mimicking gel phantoms exposed to the field of a 2.0-MHz high-intensity focused ultrasound (HIFU) transducer. We observed that boiling bubbles were generated in a localized heated region and cavitation clouds were subsequently induced ahead of the expanding bubble. This process was repeated with HIFU pulses and eventually resulted in a tadpole-shaped lesion. A simplified numerical model describing the scattering of the incident ultrasound wave by a vapor bubble was developed to help interpret the experimental observations. Together with the numerical results, these observations suggest that the overall size of a lesion induced by boiling histotripsy is dependent on the sizes of (i) the heated region at the HIFU focus and (ii) the backscattered acoustic field by the original vapor bubble.
(E-mail: n.saffari@ucl.ac.uk)

Key Words: **High-intensity focused ultrasound, Boiling histotripsy, Boiling bubbles, Cavitation clouds.**

INTRODUCTION

High-intensity focused ultrasound (HIFU) is a non-invasive ultrasound technique that has been used to thermally necrose solid tumors without disruption to surrounding tissue (Aubry et al. 2013; ter Haar and Coussios 2007). In recent years, an alternative HIFU technique to thermal ablation has been developed. This is known as mechanical tissue fractionation or histotripsy. Acoustic peak positive (P_+) and negative (P_-) pressures at the HIFU focus used in histotripsy are comparable to those in the shockwaves used in lithotripsy for kidney stone fragmentation (Pishchalnikov et al. 2003; Zhu et al. 2002). One of the initial works to show the feasibility of using acoustic shockwaves to induce controlled mechanical injuries in soft tissue was published by Tavakkoli et al. (1997). A well-defined lesion in the form of a cavity can be produced by histotripsy without any significant thermal damage at the periphery of the cavity. Recent *in vivo* studies on kidney, prostate, heart and liver have shown that a lesion produced by histotripsy contains complete fragmentation of tissue and is sharply demarcated between treated and untreated regions (Hall et al. 2009; Khokhlova et al. 2014; Pahk et al. 2015, 2016; Roberts et al. 2006; Styn et al. 2010; Vlaisavljevich et al. 2013; Xu et al. 2010). Subcellular debris remaining inside a mechanically fractionated lesion can be absorbed as part of the physiologic healing mechanism; whereas a thermally ablated lesion becomes fibrous scar tissue (Hoogenboom et al. 2015).

In histotripsy, there are two different methods of creating pure mechanical damage of soft tissue by (i) pulsed ultrasound cavitation or (ii) shockwave heating and millisecond boiling (Canney et al. 2010a, 2010b; Khokhlova et al. 2011, 2014; Khokhlova et al. 2015; Maxwell et al. 2011; Parsons et al. 2006). In both methods, acoustic

We have no conflict of interest.

Address correspondence to: Nader Saffari, Department of Mechanical Engineering, University College London, Torrington Place, London WC1E 7JE, United Kingdom. E-mail: n.saffari@ucl.ac.uk

[1] Current affiliation: Center for Bionics, Biomedical Research Institute, Korea Institute of Science and Technology (KIST), Seoul 02792, Republic of Korea.

cavitation is believed to be one of the main mechanisms for inducing mechanical tissue fractionation (Khokhlova et al. 2015). An inertial cavitation cloud at the HIFU focus can be formed by two different mechanisms, referred to as shock scattering histotripsy and intrinsic threshold histotripsy (Allen and Hall 2015; Vlaisavljevich et al. 2016). For shock scattering histotripsy, several microsecond-long HIFU pulses with high peak positive ($P_+ > 80$ MPa) and negative ($P_- = 15–25$ MPa) acoustic pressures at the focus are used to produce a dense bubble cloud. This cloud formation results from the production of a greater peak negative pressure field generated by the interference between the reflected and inverted peak positive pressure from a single cavitating bubble and the incoming incident rarefactional phase (Maxwell et al. 2011; Vlaisavljevich et al. 2014). In intrinsic threshold histotripsy, a single microsecond-long HIFU pulse with a single dominant negative pressure P_- of 24–30 MPa at the focus is employed to induce a cavitation cluster directly from the negative pressure phase of the incident acoustic wave (Lin et al. 2014; Maxwell et al. 2013; Vlaisavljevich et al. 2015a, 2015b). Because the pressure threshold for cavitation clouds is –28 MPa for most soft tissues (Lin et al. 2014; Maxwell et al. 2013), the site of the bubble cloud is spatially confined to the HIFU focus.

In contrast to shock scattering or intrinsic threshold histotripsy, another method of inducing a mechanically fractionated lesion exists. This ultrasound technique is known as boiling histotripsy, which utilizes shockwave heating to produce a boiling vapor bubble (as opposed to cavitation clouds) and fractionate soft tissue with a number of millisecond HIFU pulses (Khokhlova et al. 2015). Boiling histotripsy has been demonstrated in *ex vivo* bovine liver (Khokhlova et al. 2011; Wang et al. 2013), heart (Wang et al. 2013), kidney (Schade et al. 2014) and *in vivo* porcine and rat liver (Khokhlova et al. 2014; Pahk et al. 2015, 2016). These studies have shown that boiling histotripsy can induce similar lesions to those generated by shock scattering histotripsy or intrinsic threshold histotripsy.

Mechanisms involved in boiling histotripsy are currently being investigated by several research groups such as Canney et al. (2010a), Khokhlova et al. (2011), Kreider et al. (2011), Wang et al. (2013) and Simon et al. (2012, 2015). In soft tissue, significant acoustic wave distortion at the HIFU focus because of tissue non-linearity leads to the production of a shock wavefront. This wavefront contains tens of higher-order harmonic components of the fundamental frequency. Because the absorption of ultrasound energy in tissue increases with frequency (ter Haar and Coussios 2007), a shockwave enables the heating rate to be increased dramatically. Canney et al. (2010a) demonstrated that localized heating by shockwaves at the HIFU focus can raise tissue temperature to 100°C in a few milliseconds, resulting in the formation of a boiling vapor bubble at the HIFU focus. This bubble then grows to millimeter size, which may tear off tissue because of shear stresses produced around the oscillating bubble (Khokhlova et al. 2011). The growth of this millimeter-sized bubble, known as rectified bubble growth, is likely to occur because of the combination of the asymmetry in the compressional and rarefactional pressure phases in the shock waveforms and water vapor transport (Kreider et al. 2011). After the formation and explosive growth of a boiling bubble, it further interacts with incoming incident shockwaves to promote a mechanical tissue fractionation process (Maxwell et al. 2012). A miniature acoustic fountain and atomization may occur at the tissue-bubble interface to emit jetting with sub-micrometer–sized tissue fragments into the bubble (Simon et al. 2012).

In general, the shape of a lesion produced by boiling histotripsy is tadpole like, consisting of a head and a tail with the head closest to the HIFU source (Khokhlova and Hwang 2011). Canney et al. (2010b) and Khokhlova et al. (2011) observed that the HIFU focus was at the tail and the head had migrated toward the HIFU transducer during boiling histotripsy. Khokhlova et al. (2011) and Simon et al. (2012) suggested that the production of a head-shaped lesion is likely to be a result of the formation of a boiling bubble at the HIFU focus and the HIFU atomization at the tissue-bubble interface. Besides this, the tail of a lesion may be formed by streaming of the liquefied tissue within the forming head (Wang et al. 2013). These proposed mechanisms, however, are not enough to explain the prefocal shift of the lesion head toward the transducer, because the atomization process is likely to be limited to the region where shocks and boiling bubbles are present (Khokhlova et al. 2011; Wang et al. 2013). Therefore, other mechanisms may be involved in boiling histotripsy besides the HIFU atomization and the streaming effects.

Although several studies have demonstrated the efficacy of boiling histotripsy for fractionating tumors, the exact mechanisms underpinning this phenomenon are poorly understood, particularly the interaction of a boiling bubble with incoming incident shockwaves. To that end, the main objective of the present study is to provide a better understanding of the mechanisms behind the formation of a mechanically induced tadpole-shaped lesion resulting from boiling histotripsy. In this study, a high-speed camera and a passive cavitation detection (PCD) system are used to observe the dynamics of bubbles induced in tissue-mimicking gel phantoms exposed to HIFU fields and to record the corresponding acoustic emissions. Furthermore, a numerical model describing the incidence of ultrasonic waves on a vapor bubble close to the focus of the HIFU transducer and the backscattered field by the bubble, is developed using a boundary element method (BEM).

MATERIALS AND METHODS

HIFU experimental arrangement

A schematic diagram of the experimental setup used in this study is shown in Figure 1. The experiment was performed in an acrylic water bath filled with degassed and de-ionized water at a temperature of 20°C. A water treatment system (Precision Acoustics Ltd., Dorset, UK) was used for degassing. A 2.0-MHz single element bowl-shaped HIFU transducer (Sonic Concepts H106, Bothell, WA, USA) with an aperture size of 64 mm, a focal length of 62.6 mm and lateral and axial full width half maximum (FWHM) pressure dimensions of 1.05 mm and 6.67 mm was used. The HIFU transducer was characterized in our previous study (Pahk et al. 2016) using a calibrated 0.2-mm polyvinylidene fluoride (PVDF) needle hydrophone (Precision Acoustics Ltd.) in water (free-field) under linear propagation conditions. The HIFU source was driven by a function generator (Agilent 33220A, Santa Clara, CA, USA) *via* a linear radiofrequency (RF) power amplifier (ENI 1040 L, Rochester, NY, USA). A computer with waveform generation software (Agilent Waveform Builder, CA, USA) was used for driving the function generator with the desired HIFU pulsing protocol. A power meter (Sonic Concepts 22A, Bothell, WA, USA) was connected between the RF power amplifier and the HIFU source to measure the level of the electrical power P_{elect} supplied to the transducer.

During the experiments, the position of the HIFU transducer was fixed relative to the phantom in the water bath and an acoustic absorber (AptFlex F28, Precision Acoustics Ltd.) was placed on the opposite end to minimize ultrasonic reflections. A 10-MHz focused PCD (20 mm in diameter and 64 mm in geometric focal length, Sonic Concepts Y107) featuring a wide bandwidth (10 kHz–20 MHz) was connected to a digital oscilloscope (LeCroy HDO 6054, Berkshire, UK). This PCD was used to obtain acoustic emissions resulting from cavitation activity at the HIFU focus. A sampling frequency of 0.5 GHz was used.

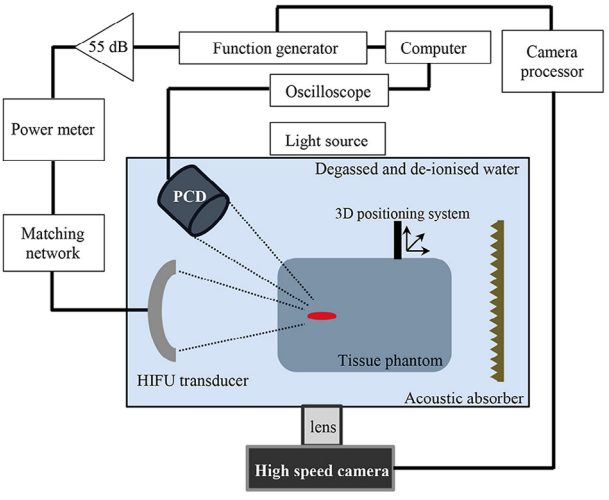

Fig. 1. HIFU experimental setup used for investigating the generation of tadpole-shaped lesions resulting from boiling histotripsy. HIFU = high-intensity focused ultrasound.

Table 1. Composition of 50 mL gel with 7% concentration of BSA

Components	Quantity	Percent (%)
Degassed and de-ionized water	35.805 mL	71.61
BSA	3.5 g	7
1 M TRIS	5 mL	10
40% Acrylamide	8.75 mL	17.5
10% APS	0.42 mL	0.84
TEMED	0.025 mL	0.05

BSA = bovine serum albumen; TRIS = tromethamine; APS = ammonium persulfate; TEMED = tetramethylethylenediamine.

Tissue-mimicking gel phantoms

An optically transparent-tissue mimicking phantom containing a polyacrylamide gel with bovine serum albumin (BSA) used in this study has also been used in a number of other boiling histotripsy studies (Canney et al. 2010a; Khokhlova et al. 2011; Zhou and Gao 2013). Temperatures >60°C cause BSA protein to denature and form an opaque thermal lesion, which can be visualized. Table 1 shows the chemical composition required to produce a 50-mL gel with 7% BSA concentration. A tissue phantom consisting of the chemical composition listed in Table 1 has similar acoustic and thermal properties to those of liver, except for the attenuation coefficient, which is 0.15 dB cm^{-1} MHz^{-1}, rather than that for liver, which is 0.52 dB cm^{-1} MHz^{-1} (Khokhlova et al. 2011; Lafon et al. 2005).

The tissue phantom was prepared by first mixing 3.5 g of BSA (Sigma-Aldrich A7906, Dorset, UK) in 35.805 mL of degassed and de-ionized water. The mixture was gently stirred to dissolve the BSA completely. The solution was then placed in a vacuum chamber (Edwards High Vacuum ISC30A, Sussex, UK) and held in a vacuum of 720 mm Hg for 30 min for additional degassing. A total of 8.75 mL of acrylamide (Sigma-Aldrich A9926) was added to the mixture followed by a 1 mol L^{-1} TRIS buffer (Sigma-Aldrich T2694) and 0.42 mL of ammonium persulfate (Sigma-Aldrich A7460) to initiate polymerization. Because acrylamide is a neurotoxic substance, the mixing process was performed in a fume hood (Labcaire T400L, Somerset, UK) with appropriate safety measures. The entire solution was again stirred gently and placed in the vacuum chamber with a vacuum of 720 mm Hg for 1 hour. Finally, 0.025 mL of TEMED (Sigma-Aldrich T9281) was added to the solution to accelerate the polymerization process. The final solution was immediately poured into a customized mold (6 × 6 × 6 cm). Because the polymerized gel has a limited lifespan of several weeks (Khokhlova et al.

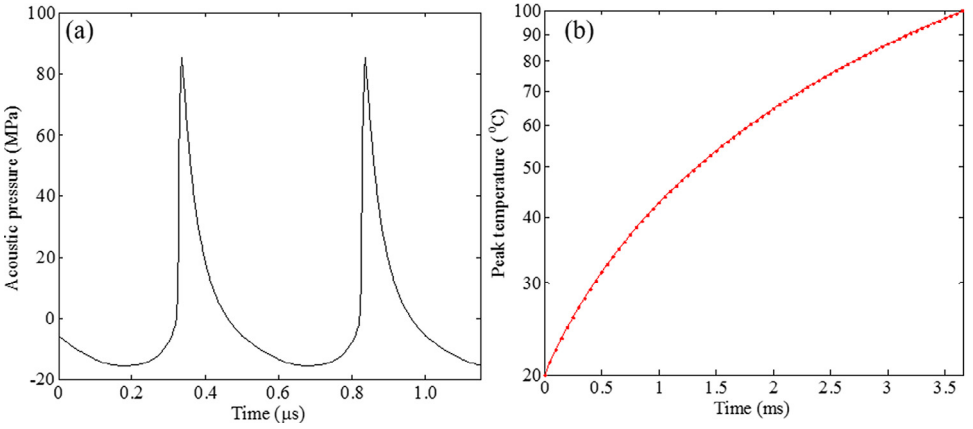

Fig. 2. Simulated acoustic waveforms and peak temperatures at the HIFU focus in the tissue phantom. (a) Acoustic wavefronts with $P_{elect} = 200$ W ($P_+ = 85.4$ MPa, $P_- = -15.6$ MPa at focus). (b) Corresponding peak temperature. The time to reach the boiling temperature of 100°C is predicted to be 3.66 ms. HIFU = high-intensity focused ultrasound.

2006), it was stored in an air-tight plastic bag at 8°C and used the next day for experiments.

Before we performed the camera experiments, the tissue phantom was kept at room temperature until its temperature reached 20°C. The phantom was then cut into cuboid samples (1.5 × 3 × 6 cm) and clamped in a custom-built holder (4.5 × 5 × 7.5 cm). The holder, coupled with the phantom, was attached to a customized 3-axis positioning system for alignment with the HIFU focus. The distance from the center of the transducer surface to the phantom was 57.6 mm. Therefore, the HIFU focus was 5 mm below the surface of the phantom. This depth was chosen according to our previous *in vivo* study (Pahk et al. 2016) that shows the production of a well-defined tadpole-shaped lesion at 5 mm below the surface of the liver without rupturing the liver surface. A total of 17 tissue phantoms ($n = 17$) was used in this study.

Camera setup

A high-speed camera (FASTCAM-ultima APX, Photron, San Diego, CA, USA) with a 12 X Navitar lens (Navitar, Rochester, NY, USA) connected to a 3-axis-positioning system (Sherline Products 5430, Vista, CA, USA) was used to film the bubble dynamics induced at the HIFU focus in the tissue phantom. The camera was operated at 1000, 15,000 and 100,000 frames per second (fps) with a shutter speed of 1/1000 s, 1/15,000 s and 1/100,000 s, and a pixel resolution of 512 × 128, 1028 × 128 and 128 × 32, respectively (24 μm/pixel). During the experiments, 15,000 and 100,000 fps were used to capture bubble dynamics induced by 1 HIFU pulse or 5 HIFU pulses in the gel while 1000 fps was employed for 50 HIFU pulses because of memory limitation. All experiments were backlit with an illuminating system (Solarc ELSV-60, General Electric Company, Fairfield, CT, USA). Hence, captured optical images appeared as shadowgraphs where the tissue phantom appeared grey and HIFU-induced bubbles appeared black. Optical images were post-processed with Photron FASTCAM Viewer (Photron). Tissue phantoms were cross-sectioned after HIFU exposure for morphologic analysis.

During the experiments, a camera processor (FASTCAM-ultima APX, Photron) triggered the camera and the function generator at the same time to synchronize the image capturing process and HIFU exposure.

HIFU exposure condition

A 10 ms-long HIFU pulse with $P_{elect} = 200$ W (nominal electrical to acoustic power conversion efficiency of 85%, $P_+ = 85.4$ MPa and $P_- = -15.6$ MPa) was used to produce a lesion in the tissue phantom. The duty cycle (1%) and the pulse repetition frequency (1 Hz) were kept constant while changing the number of pulses, which was set to 1, 5 or 50. In boiling histotripsy, it has been shown that the time to initiate boiling at the HIFU focus can be reliably predicted theoretically (Canney et al. 2010a; Khokhlova et al. 2011; Wang et al. 2013). Acoustic peak positive (P_+) and negative (P_-) pressures at the HIFU focus in the gel were, therefore, obtained by numerically solving the Khokhlov-Zabolotskaya-Kuznetsov (KZK) parabolic non-linear wave propagation equation for a set of input parameters using the HIFU Simulator v1.2 (Soneson 2009). The simulated acoustic waveform at the focus is shown in Figure 2a. Figure 2b depicts the corresponding peak temperature rise. This was calculated using the bioheat transfer (BHT) equation (Pennes 1948) and the time to reach the boiling temperature of 100°C (t_b) was predicted to be 3.66 ms. The physical properties of the tissue phantom used in the simulations are listed in Table 2. The HIFU exposure parameters used in this study were verified for the creation of a cavity with *in vivo* experiments reported

Table 2. Properties of tissue phantom used in the acoustic and temperature fields simulations

Properties	Value*
Speed of sound	1544 m s^{-1}
Mass density	1044 kg m^{-3}
Absorption coefficient at 1 MHz	15 dB m^{-1}
Coefficient of non-linearity	4.0
Specific heat capacity per unit volume	5.3×10^6 J m^{-3} °C^{-1}
Thermal diffusivity	1.3×10^{-7} m^2 s^{-1}
Ambient temperature	20°C

* Obtained from Khokhlova et al. 2011.

earlier (Pahk et al. 2015, 2016) and were similar to those used by Khokhlova et al. (2011).

Scattered pressure fields

The presence of a vapor bubble close to the focus of the HIFU transducer is likely to cause scattering of the incident ultrasonic field because of the difference in the acoustic impedance between water vapor and the tissue phantom. This phenomenon may lead to constructive and destructive interactions of the scattered field with the incident field, potentially generating localized peak negative pressures, leading to additional cavitation nucleation sites. Furthermore, the presence of a vapor bubble close to the transducer focus may also lead to a distortion of the focus and generate a shadow zone.

It is well-known that the KZK equation can only simulate one-way paraxial propagation. Producing a full-wave non-linear acoustic propagation model capable of dealing with scattering by localized heterogeneities remains a challenge. This is particularly the case if the computational domain is large relative to the wavelength of the highest frequency present in the ultrasonic signal. On the basis of the KZK simulations, significant harmonic content is present at the focus up to 10 MHz. This is likely to result in a densely meshed computational grid. It is, therefore, likely that accurately modelling such a configuration will present substantial computational challenges. To get a qualitative appreciation of what the effects of scattering of the incident HIFU field by a vapor bubble may be, a linear scattering analysis was, therefore, chosen. The calculated scattered acoustic pressure fields based on the linearity assumption would therefore only be for qualitative analysis. BEMs are particularly well-suited to dealing with exterior scattering problems, and such analysis techniques will be chosen here. In BEM, the partial differential equation to be solved is reformulated into an integral equation that is defined on the boundary of the domain (in this case, on the surface of the vapor bubble) and an integral that relates the boundary solution to the solution at any point in the domain. The boundary integral equation may then be solved by discretizing the surfaces defined by the domain boundaries into smaller regions known as boundary elements. A major advantage of BEM over other numerical schemes, such as finite difference time domain methods, is that the discretization occurs only over the surfaces rather than over the entire domain. More details on BEM are provided by Banerjee (1994).

The BEM implementation used in this study was described by Gélat et al. (2014, 2015). The method is a colocation BEM implementation of the Kirchhoff-Helmholtz integral equation, which uses iso-parametric elements with quadratic shape functions. The scatterer is assumed to be locally reacting so that $\partial p / \partial n = i\omega\rho_v u_n$ on the surface of the vapor bubble, where p is the acoustic pressure in the liquid, n is the node on the mesh of the surface, u_n is the normal component of the particle velocity vector, ρ_v is the liquid density, ω is the angular frequency and $i^2 = -1$. Transmission of acoustic waves through the bubble was neglected, because of the significant difference between the acoustic impedance of water vapor and that of the tissue phantom (Canney et al. 2010a).

For computation of scattered acoustic fields from a boiling bubble, the BEM scheme requires an incident acoustic pressure field on the surface of the scatterer as input data. This was derived using a Rayleigh integral method (Pierce 1989) by effectively discretizing the surface of the HIFU source into smaller surfaces with a point source located at their centroid. By weighting each source with the appropriate surface area and by summing all their contributions, the incident field at any required location may be computed. This is achieved through a discretization of the following integral:

$$p(\vec{r}, t) = \frac{i\rho ck}{2\pi} e^{i\omega t} \iint_s \frac{e^{-ik\|\vec{r}-\vec{r}_0\|}}{\|\vec{r}-\vec{r}_0\|} \vec{u}\cdot\vec{n} dS \qquad (1)$$

where ρ is the density of the tissue phantom, $k = \omega/c$ is the acoustic wave number and c is the sound speed in the phantom. $\vec{r}$ depicts a position vector in the acoustic domain, $\vec{r}_0$ is a position on the surface of the source, $\vec{n}$ is the unit normal vector on the surface of the source (pointing toward the focus), $\vec{u}$ is the velocity and s is the radiating surface of the HIFU source, which is assumed to be moving uniformly in the radial direction.

The exterior domain was assumed to be homogeneous, possessing the properties of the tissue phantom gel. In fact, this domain also comprises a region of water between the HIFU source and the gel. This water region was not included here, and the normal surface velocity of the transducer was adjusted to result in 22 MPa at the focus, in the absence of the scatterer. The pressure value of 22 MPa was obtained from the simulated acoustic pressure for the first harmonic using the KZK simulation (*i.e.,* in the linear case). The resulting acoustic pressure at focus is shown in Figure 3b, which represents the sum of the

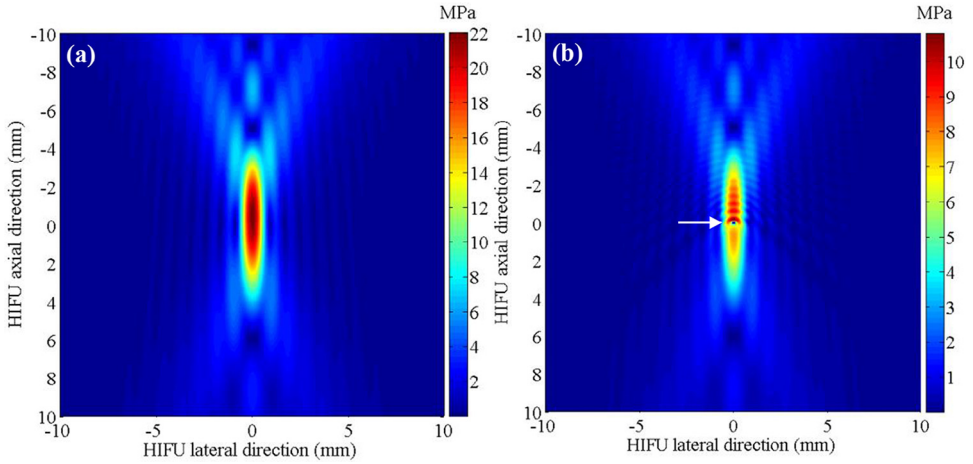

Fig. 3. Simulated acoustic pressure magnitudes at the HIFU focus using BEM. The contour plots of the incident acoustic pressure (a) without and (b) with a scatterer. The presence of a vapor bubble is indicated by an *arrow* in (b). The HIFU beam propagates from top to bottom. HIFU = high-intensity focused ultrasound; BEM = boundary element method.

incident and the scattered pressure magnitude from a vapor bubble.

RESULTS

Formation of a boiling bubble in the tissue phantom gel with a single HIFU pulse

Figure 4 shows a sequence of camera images obtained during a single 10-ms HIFU pulse in the tissue-mimicking gel phantom with an acoustic power of 170 W (P_+ = 85.4 MPa; P_- = −15.6 MPa at the HIFU focus). Localized heating in the HIFU focal region is observed as a dark elliptical shape at 3.4 ms (Fig. 4b). This heated region corresponds well to the simulated temperature contour plot shown in Figure 4c. A large bubble of 360 μm in diameter appears in this heated region after 3.6 ms of exposure to the HIFU field (indicated by an *arrow* in Fig. 4d). This bubble is hereafter referred to as a boiling bubble because its onset time matches the calculated time to reach a boiling

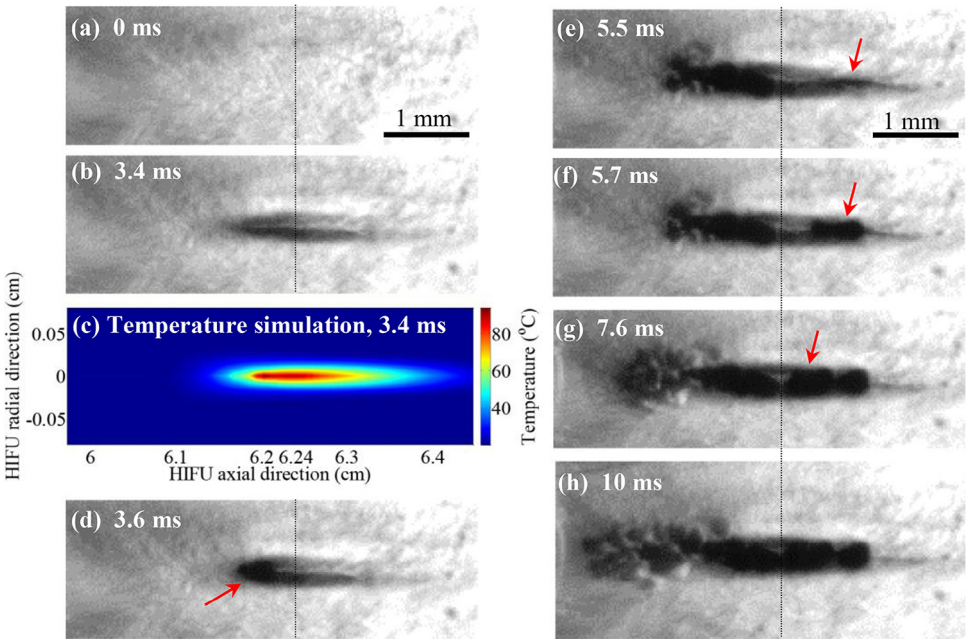

Fig. 4. A sequence of high-speed camera images (a, b, d–h) obtained in an optically transparent tissue phantom during the single 10-ms HIFU insonation with an acoustic power of 170 W (P_+ = 85.4 MPa; P_- = −15.6 MPa at the HIFU focus). Images were captured at a 15,000 fps. (c) Simulated temperature contour plot at t = 3.4 ms. The HIFU beam propagates from left to right. The vertical lines pass through the HIFU focal point perpendicular to the beam axis. The time at 0 ms corresponds to the start of the HIFU exposure. HIFU = high-intensity focused ultrasound; fps = frames per second.

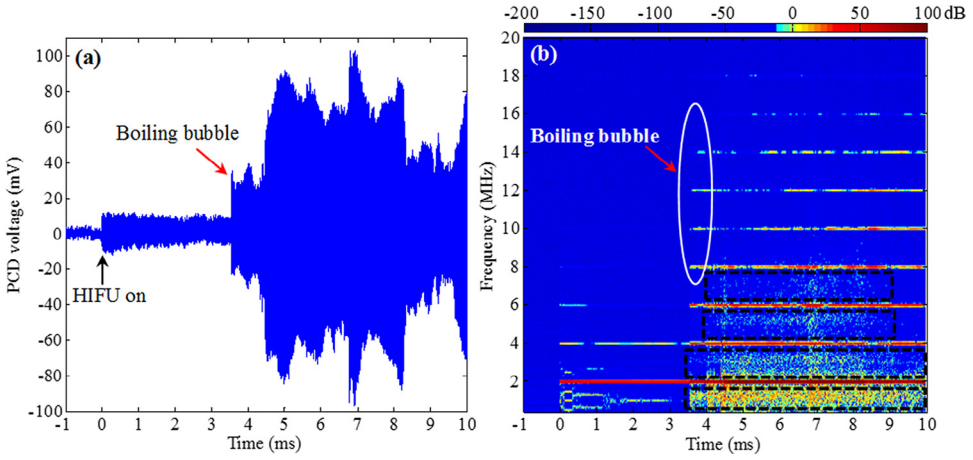

Fig. 5. Acoustic signal emitted from the HIFU focus in the gel during the single 10-ms HIFU pulse. (a) The PCD voltage versus time plot and (b) the corresponding spectrogram. Acoustic emissions were recorded at a sampling rate of 0.5 GHz. The time at 0 ms represents the start of the HIFU insonation. HIFU = high-intensity focused ultrasound; PCD = passive cavitation detection.

temperature of 100°C (t_b = 3.66 ms) (Khokhlova et al. 2011). A significant increase in the PCD voltage occurs as this large boiling bubble manifests itself. This can be seen in the PCD voltage versus time plot in Figure 5a. Also coinciding with the appearance of this bubble is the manifestation of higher order multiple harmonic components of the fundamental frequency (2 MHz) in the spectrogram in Figure 5b. These significant changes are indications of the formation of a boiling bubble because of the reflection of an incident non-linear–shocked wave from this bubble (Canney et al. 2010a).

During the experiments, the time to boiling for the single HIFU pulse in the gel was 3.78 ± 0.67 ms (mean ± standard deviation SD with n = 17) with differences of 0.12 ms between the PCD measurement and the temperature simulation.

After the formation of a boiling bubble at t = 3.6 ms (see Fig. 4d), a cavitation cluster is subsequently produced in front of the boiling bubble, progressing toward the HIFU source until the HIFU pulse is switched off (see Fig. 4e–h). Simultaneously with the generation of the bubble cloud, a significant appearance of broadband emissions (an indicator of inertial cavitation) is noticed within the black dashed lines in the corresponding spectrogram plotted in Figure 5b. In addition to the generation of a cavitation cluster, a secondary localized heated region at ~1 mm away from the primary boiling bubble further along the beam axis is observed. This event is indicated by an *arrow* in Figure 4e and is followed by the production of a secondary boiling bubble at t = 5.7 ms, also indicated by an *arrow* in Figure 4f. More boiling bubbles can be seen to form at t = 7.6 ms toward the primary boiling bubble (see Fig. 4g). These secondary boiling bubbles are spatially confined to the localized heated region.

Formation of a tadpole-shaped lesion with multiple HIFU pulses

Five HIFU pulses. Figure 6 shows a series of high-speed camera images taken during five 10 ms HIFU pulses. Images in the left column represent the formation of a boiling bubble during each HIFU pulse (indicated by *arrows* in Fig. 6a), whereas those in the middle column show bubble activities at the end of each HIFU pulse (see Fig. 6b). During each HIFU pulse, a boiling bubble appears either at the HIFU focus or close to the focus (within 1 mm, see Fig. 6a), but disappears in the time interval between HIFU pulses (1% duty cycle). The time taken to form a boiling bubble decreases with HIFU pulses (3.6, 3.1, 2.9, 2.5 and 2.3 ms). Besides this boiling bubble, a cavitation bubble cloud is always produced in front of a boiling bubble (indicated by the *blue arrows* in Fig. 6b), persisting throughout each HIFU exposure, but disappearing between HIFU pulses.

The corresponding induced mechanical damage in the gel before the arrival of the next HIFU pulse is shown in the right column in Figure 6c. Examining the phantom morphology at the HIFU focus, residual mechanical damage of the gel is optically visible and the size of the lesion becomes enlarged with the number of HIFU pulses. When comparing the location of the bubbles (*i.e.,* boiling bubbles and cavitation clouds) with the corresponding residual damage induced in the phantom (see Fig. 6b and c), the position of the head-shaped lesion corresponds well to that of the cavitation cloud; whereas the boiling bubbles generated in the heated region match the location of the tail-shaped lesion. In addition, bubbles smaller than 200 µm in diameter are pushed away from the HIFU focus (indicated by the *black arrows* in Fig. 6b) most probably because

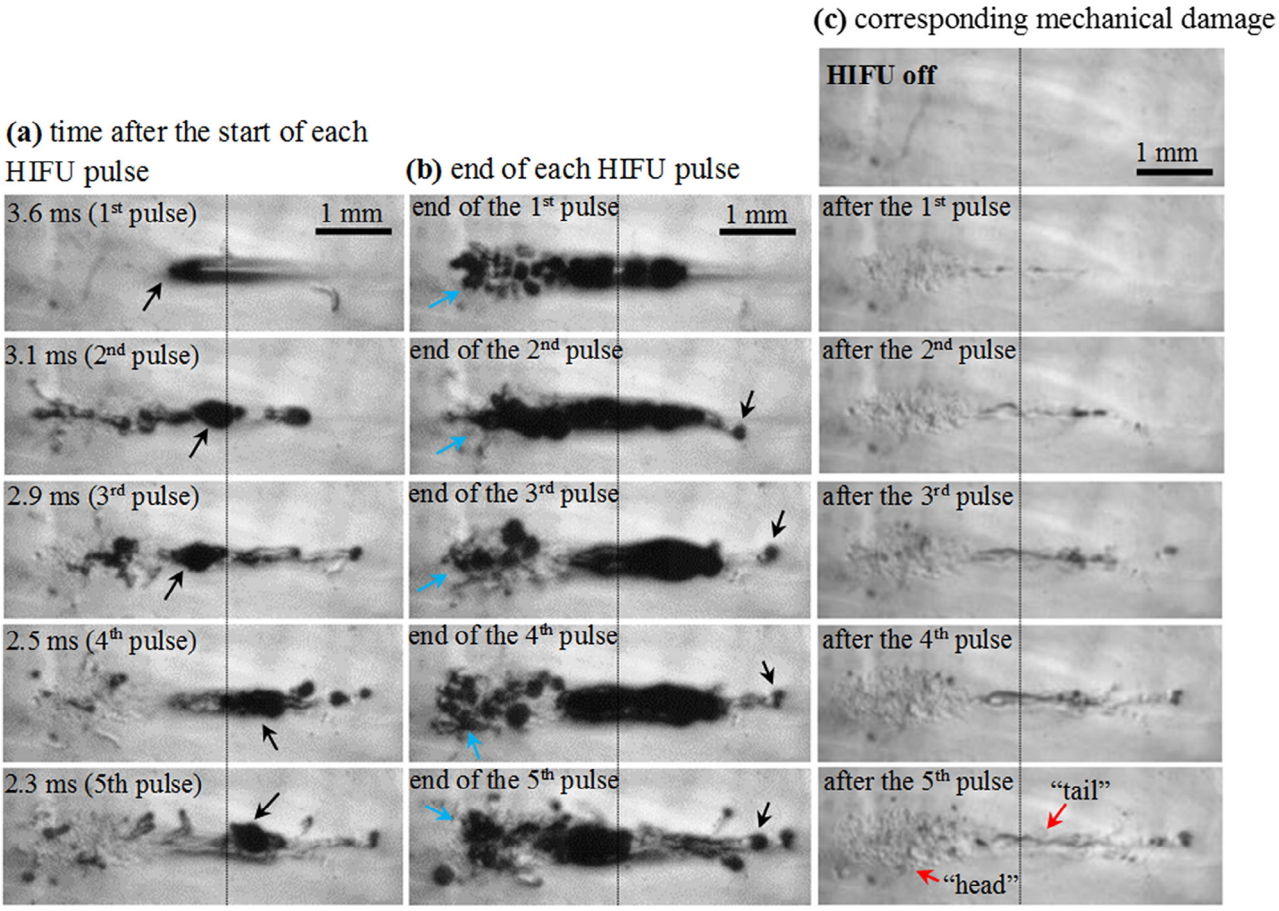

Fig. 6. High-speed images taken during five HIFU pulses. (a) Formation of a boiling bubble during each HIFU pulse (*left column*). (b) The end of each pulse (*middle column*). (c) Corresponding mechanical damage induced in the gel before the arrival of the next HIFU pulse (*right column*). The HIFU beam propagates from left to right. The images were captured at a frame rate of 15,000 fps. The vertical lines pass through the HIFU focal point perpendicular to the beam axis. HIFU = high-intensity focused ultrasound; fps = frames per second.

of the HIFU radiation force. This movement may also contribute to the formation of the tail together with the generation of boiling bubbles.

50 HIFU pulses. In boiling histotripsy, 10–50 HIFU pulses are usually delivered to produce a well-defined mechanically fractionated lesion (Maxwell et al. 2012). Figure 7 shows several high-speed images captured during 50 HIFU pulses. The shape of a tadpole-like mechanical damage produced in the phantom corresponds well to the locations of a cavitation cloud and of boiling bubbles in the head and in the tail, respectively. This is further confirmed by cross-sectioning the lesion immediately after exposure to the 50th HIFU pulse, as shown in Figure 7f and g. No evidence of thermal damage, which would manifest itself as an opaque lesion (Khokhlova et al. 2011), was present.

Figure 8 shows the length along the direction of wave propagation and the width in the lateral direction of the head and of the tail as a function of the HIFU pulse numbers. After the 5th HIFU pulse, the length of the head does not increase significantly; whereas the width of the head and both the width and length of the tail continue to grow. After the 30th HIFU pulse, the overall lesion size does not change significantly.

DISCUSSION

Formation of a boiling bubble

In this work, the mechanism for the formation of a tadpole-shaped lesion produced by boiling histotripsy was investigated both experimentally and numerically. Canney et al. (2010a) and Khokhlova et al. (2011) showed that localized shockwave heating can increase the temperature to 100°C in a few milliseconds, resulting in the formation of a boiling vapor bubble at the HIFU focus. The experimental results presented in this study concurred with those of Canney et al. (2010a) and Khokhlova et al. (2011). A boiling bubble appeared in a localized heated region (Fig. 4). The boiling time resulting from a single 10-ms HIFU pulse in the gel (3.78 ± 0.67 ms, mean ± SD with $n = 17$) agreed well with findings obtained from the

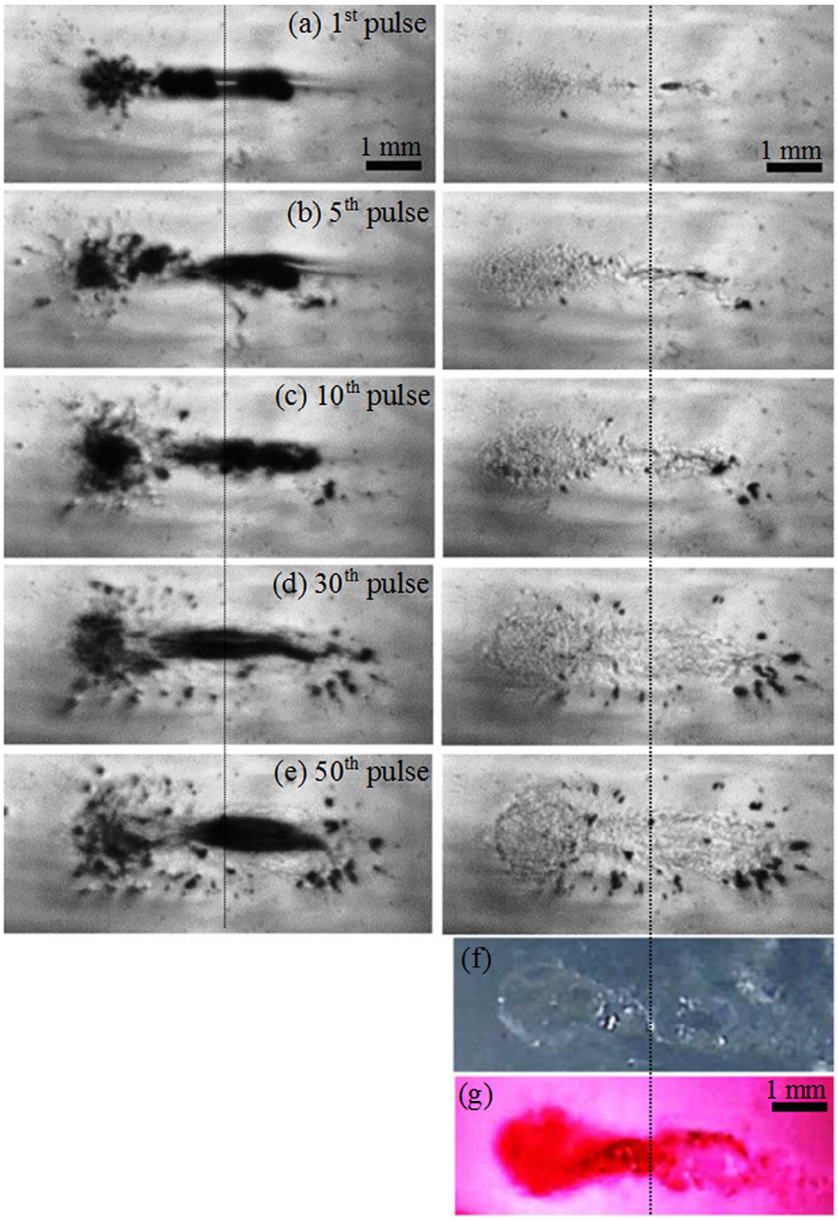

Fig. 7. High-speed images taken over the course of 50 HIFU pulses (a–e). (f) Cross-sectioned lesion after the 50th HIFU pulse and (g) the same lesion as (f), but with an added dye. An acquisition rate of 1000 fps was used. Bubble activity at the end of each 10-ms HIFU pulse (*left column*) and the corresponding mechanical damage induced in the gel (*right column*), which were taken at 1 ms (*i.e.,* 1 frame) before the arrival of the next HIFU pulse. The HIFU beam propagates left to right. The vertical dashed lines pass through the HIFU focal point perpendicular to the beam axis. HIFU = high-intensity focused ultrasound.

temperature simulation, where the computed time to boil was predicted to be 3.66 ms. Furthermore, it was observed that the onset time of a boiling bubble reduced with the number of HIFU pulses used (Fig. 6). This is most likely to be because of an accumulation of heat at the HIFU focus, where the peak temperature does not return to ambient temperature between pulses (Khokhlova et al. 2011; Zhou and Gao 2013).

During the HIFU exposure, the changes in temperature-dependent acoustic properties, especially speed of sound, can lead to a shift of the HIFU focus in the axial direction toward the transducer (Hallaj et al. 2001). Figures 4d and 6a show that a boiling bubble forms at the edge of the heated region during the first 10-ms HIFU pulse. This was also observed by Khokhlova et al. (2011). In the presence of a localized region heated by shockwaves,

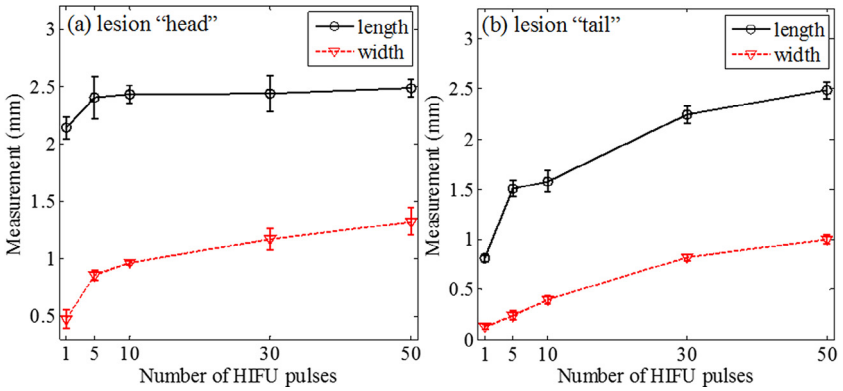

Fig. 8. Length measurement (mean ± SD) along the direction of wave propagation and the width along the lateral direction of the head and of the tail as a function of the number of HIFU pulses. The reference measurement point was at the HIFU focus. Photron FASTCAM Viewer software (Photron, San Diego, CA, USA) was used for the size measurement (24 μm/pixel). Each measurement was repeated five times. HIFU = high-intensity focused ultrasound.

a large temperature gradient exists across the edge of the region. This eventually leads the local speed of sound in the heated volume to be greater than that outside of this region, causing an acoustic refraction effect at the interface.

Interaction of a boiling bubble with an incident shockwave

Maxwell et al. (2011) showed that the reflection and inversion of incident shockwaves from the surface of a single cavitating bubble produces a large peak-negative pressure field, leading to additional bubble nucleation sites for cavitation clouds. This phenomenon is known as the shock scattering effect. This cavitation cluster was also observed during the boiling histotripsy, after the creation of a boiling bubble at the HIFU focus (Fig. 4e–h). Simultaneously with the bubble cloud formation in front of a boiling bubble, a secondary localized heated region appears within the HIFU focal region, resulting in a secondary boiling bubble (Fig. 4e, f). This is likely because (i) the incident acoustic field is partially shielded by the cavitation cluster together with the boiling bubble and (ii) the larger size of the HIFU focal width (FWHM of 1.05 mm) relative to that of the region heated by shocks (~0.2 mm; Fig. 4c). Indeed, because of constructive and destructive interference between the incident field and that scattered by the secondary boiling bubble, local pressure minima as well as enhanced heating may be induced. This may lead to the generation of a number of boiling bubbles in front of the secondary boiling bubble moving toward the transducer (Fig. 4f–h). Figure 9 shows the simulated sum of the incident pressure and the pressure scattered by a boiling vapor bubble. The backscattered acoustic pressure field in front of the bubble and the reduced acoustic pressure in the shadow zone behind the bubble can be observed clearly. The boundary element numerical results have been obtained based on the linearity assumption. So, although both the backscattered acoustic field and the field behind the bubble are given by the simulations, it is only the pressure field behind the bubble that can be used for a direct comparison with the experimental observations. This is because the dominant components in the backscattered field of an incident shock from a bubble have been experimentally observed to be the higher frequency components (Maxwell et al. 2012). The linear model used here does not model a shock or the higher harmonics of

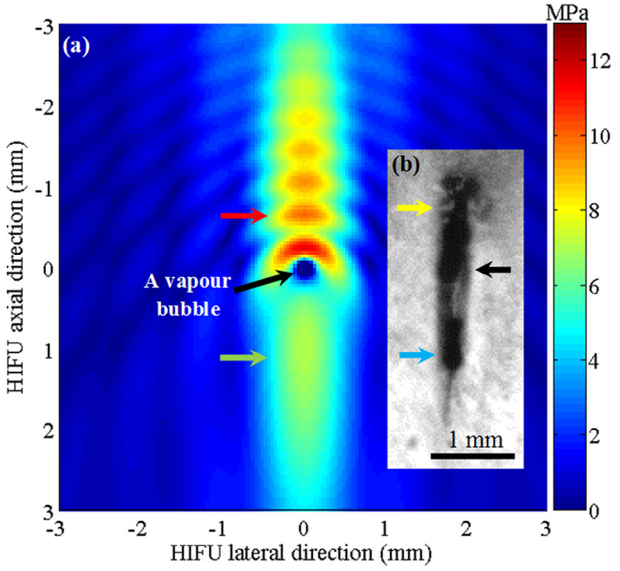

Fig. 9. (a) Calculated acoustic pressure magnitudes resulting from the scattering of the HIFU field by a boiling bubble. The presence of partially shielded acoustic pressure field behind the vapor bubble (*green arrow*). The backscattered pressures (*red arrow*). The HIFU beam propagates from top to bottom. (b) High-speed image showing a cavitation cluster (*yellow arrow*) in front of and a secondary boiling bubble (*blue arrow*) behind the primary boiling bubble (*black arrow*). HIFU = high-intensity focused ultrasound.

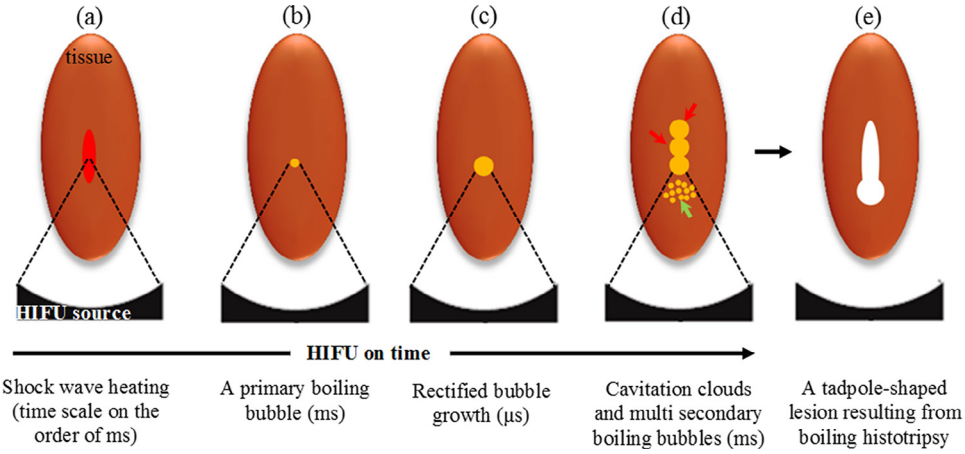

Fig. 10. Proposed mechanisms for boiling histotripsy. (a) Shockwave heating. (b) Formation of a primary boiling bubble at the HIFU focus. (c) Rectified growth of a boiling bubble. (d) Production of cavitation clouds (*green arrow*) and secondary boiling bubbles (*red arrows*). (e) Creation of a tadpole-shaped lesion resulting from boiling histotripsy. HIFU = high-intensity focused ultrasound.

the fundamental component. The fundamental component, which is the only component modelled here and the lower frequency harmonics in a shock are, however, expected to be scattered more weakly and thus more in the forward direction, that is, behind the bubble. Therefore, behind the first large vapor bubble, the simulated field can be expected to be more accurate and thus used to explain the occurrence of the secondary boiling vapor bubbles within the HIFU focal zone.

Mechanisms for the creation of a tadpole shaped lesion

Khokhlova et al. (2011), Simon et al. (2012) and Wang et al. (2013) proposed that the formation of a tadpole-shaped lesion produced by boiling histotripsy is most likely to be because of the explosive growth of a boiling bubble together with the HIFU atomization for a head-shaped lesion and the streaming of a mechanically fractionated tissue within the forming head for a tail-shaped lesion. The experimental results presented in this study, however, could possibly support an additional mechanism being responsible for the formation of a tadpole-shaped lesion. The mechanical destruction of the polymer structure of the tissue phantom corresponded well to the locations of cavitation clouds for a head and boiling bubbles for a tail, respectively (Figs. 6 and 7). The shape of the lesion was further confirmed by cross-sectioning it immediately after the HIFU insonation (Fig. 7f and g). On the basis of the numerical and experimental results presented in this work, another possible mechanism for the formation of a tadpole-shaped lesion resulting from boiling histotripsy is proposed. This is shown in Figure 10. After the formation and explosive growth of a boiling bubble at the HIFU focus, the shock scattering effect leads to the production of inertial cavitation clouds (*i.e.,* violent bubble collapses) in front of the boiling bubble. These bubble clouds, which are known to be responsible for shock scattering histotripsy and intrinsic threshold histotripsy (Khokhlova et al. 2015; Maxwell et al. 2012), enable the disruption of tissue (Hall et al. 2009; Lake et al. 2008; Schade et al. 2012a, 2012b; Vlaisavljevich et al. 2013) leading to the production of the head of the lesion. In addition to this, the shear stresses produced around several boiling bubbles within a localized heated region (Khokhlova et al. 2011) may create the tail of the lesion. Simultaneously, ultrasonic atomization at the tissue-bubble interface may also contribute some extent to the production of the tail of the lesion; however, this process is spatially limited by the presence of shocks with high enough pressure amplitudes to cause tissue atomization (Khokhlova et al. 2011; Wang et al. 2013). Cavitation clouds that form right in front of the vapor cavity may weaken the tissue or gel to facilitate ultrasonic atomization process (Khokhlova et al. 2011).

Variation of the size of a lesion with the number of HIFU pulses

As shown in Figures 7 and 8, the overall size of the lesion produced by boiling histotripsy increased gradually with the number of HIFU pulses but did not change significantly starting from the 30th pulse with the HIFU exposure condition used in this study. Khokhlova et al. (2011) and Wang et al. (2013) have also observed a similar trend in the growth of a lesion size with HIFU pulses. With the proposed mechanism described in Figure 10, it is suggested that the change of a lesion dimension is primarily dependent upon the extent of a localized heated region and the pressure amplitude of backscattered acoustic fields. As a heated region broadens with an increase in the number of HIFU pulses because of the accumulation of heat, more boiling bubbles with larger sizes will form within this heated volume. These spatially

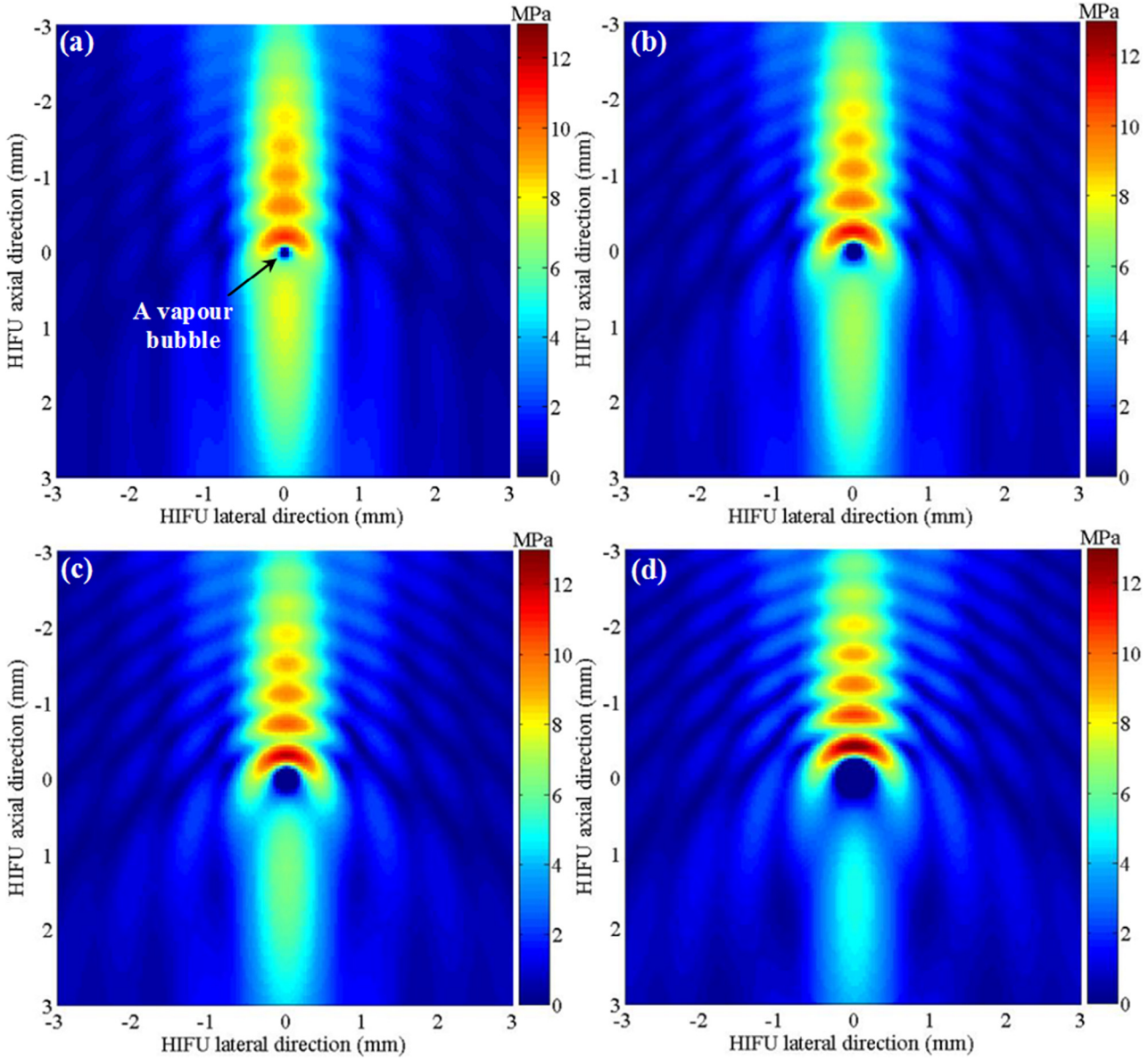

Fig. 11. The sum of the incident and the backscattered acoustic pressure magnitudes from a vapor bubble with a diameter of (a) 100 μm, (b) 200 μm, (c) 300 μm and (d) 500 μm. The HIFU beam propagates from top to bottom. HIFU = high-intensity focused ultrasound.

confined boiling bubbles lead to the formation of a tail for the lesion that grows in both axial and lateral directions along the beam axis. Simultaneously, the enlarged boiling bubble with a larger surface area generates a wider backscattered acoustic field (Fig. 11). This results in the formation of a wider cavitation cluster in the lateral direction toward the HIFU source, producing a wider head for the lesion. However, as heat transfer processes reach equilibrium between HIFU pulses, the volume over which the heating occurs reaches a maximum (Wang et al. 2013). It is, therefore, reasonable to assume that the beam width of the backscattered pressure field also reaches a maximum. As a result, the axial and lateral sizes of a tail do not change and neither does the lateral size of a head. Furthermore, the reduction of the pressure amplitude of backscattered fields due to attenuation limits the axial growth of a head toward the HIFU source. Cavitation clouds, for example, stop progressing in the direction of the HIFU transducer when the sum of incident and scattered acoustic pressures is below a pressure threshold for cavitation clouds, which is −28 MPa for most soft tissues (Lin et al. 2014; Maxwell et al. 2013). This is the most likely reason why cavitation clouds were not optically observed at the surface of the phantom during boiling histotripsy, whereby the axial extent of the resulting lesion did not rupture the surface (Fig. 7).

CONCLUSIONS

In this work, a mechanism to produce a tadpole-shaped lesion induced by boiling histotripsy was proposed and investigated. Boiling bubbles were produced in a localized heated region and cavitation clouds were subsequently induced ahead of the expanding bubble. This process was repeated and eventually resulted in a tadpole-shaped lesion. A simplified numerical model describing the scattering of the incident ultrasound wave by a vapor bubble was developed to help interpret the experimental observations. Together with the numerical results, these observations suggest that the overall size of a lesion generated by boiling histotripsy is dependent on the spatial extent of (i) the heated region at the HIFU focus and (ii) the backscattered ultrasound wave by the original vapor bubble. Future work will be focused on the prediction of the size of a mechanically induced lesion, as well as on the comparison of *ex*-and *in vivo* PCD data and induced mechanical injuries with the gel phantom at a given HIFU exposure setting.

Acknowledgments—This work was supported and funded by Department of Mechanical Engineering, University College London.

REFERENCES

Allen S, Hall T. Real-time MRI feedback of cavitation ablation therapy (histotripsy). J Ther Ultrasound 2015;3(suppl 1):O89.

Aubry JF, Pauly KB, Moonen C, Ter Haar G, Ries M, Salomir R, Sokka S, Sekins KM, Shapira Y, Ye F, Huff-Simonin H, Eames M, Hananel A, Kassell N, Napoli A, Hwang JH, Wu F, Zhang L, Melzer A, Kim YS, Gedroyc WM. The road to clinical use of high-intensity focused ultrasound for liver cancer: Technical and clinical consensus. J Ther Ultrasound 2013;1:13.

Banerjee PK. The boundary element methods in engineering. London: McGraw-Hill; 1994.

Canney MS, Khokhlova TD, Khokhlova VA, Bailey MR, Hwang JH, Crum LA. Tissue erosion using shock wave heating and millisecond boiling in HIFU fields. In: Proceedings of the 9th international symposium for therapeutic ultrasound. Laurel, MD: International Society for Therapeutic Ultrasound; 2010b. p. 36–39.

Canney MS, Khokhlova VA, Bessonova OV, Bailey MR, Crum LA. Shock-induced heating and millisecond boiling in gels and tissue due to high intensity focused ultrasound. Ultrasound Med Biol 2010a; 36:250–267.

Gélat P, ter Haar G, Saffari N. A comparison of methods for focusing the field of a HIFU array transducer through human ribs. Phys Med Biol 2014;59:3139–3171.

Gélat P, ter Haar G, Saffari N. An assessment of the DORT method on simple scatterers using boundary element modelling. Phys Med Biol 2015;60:3715–3730.

Hall TL, Hempel CR, Wojno K, Xu Z, Cain CA, Roberts WW. Histotripsy of the prostate: Dose effects in a chronic canine model. Urology 2009; 74:932–937.

Hallaj IM, Cleveland RO, Hynynen K. Simulations of the thermoacoustic lens effect during focused ultrasound surgery. J Acoust Soc Am 2001;109:2245–2253.

Hoogenboom M, Eikelenboom D, den Brok MH, Heerschap A, Fütterer JJ, Adema GJ. Mechanical high-intensity focused ultrasound destruction of soft tissue: Working mechanisms and physiologic effects. Ultrasound Med Biol 2015;41:1500–1517.

Khokhlova TD, Canney MS, Khokhlova VA, Sapozhnikov OA, Crum LA, Bailey MR. Controlled tissue emulsification produced by high intensity focused ultrasound shock waves and millisecond boiling. J Acoust Soc Am 2011;130:3498–3510.

Khokhlova TD, Hwang JH. HIFU for palliative treatment of pancreatic cancer. J Gastrointest Oncol 2011;2:175–184.

Khokhlova TD, Wang YN, Simon JC, Cunitz BW, Starr F, Paun M, Crum LA, Bailey MR, Khokhlova VA. Ultrasound-guided tissue fractionation by high intensity focused ultrasound in an *in vivo* porcine liver model. Proc Natl Acad Sci USA 2014;111:8161–8166.

Khokhlova VA, Bailey MR, Reed JA, Cunitz BW, Kaczkowski PJ, Crum LA. Effects of nonlinear propagation, cavitation, and boiling in lesion formation by high intensity focused ultrasound in a gel phantom. J Acoust Soc Am 2006;119:1834–1848.

Khokhlova VA, Fowlkes JB, Roberts WW, Schade GR, Xu Z, Khokhlova TD, Hall TL, Maxwell AD, Wang YN, Cain CA. Histotripsy methods in mechanical disintegration of tissue: Towards clinical applications. Int J Hyperthermia 2015;31:145–162.

Kreider W, Bailey MR, Sapozhnikov OA, Khokhlova VA, Crum LA. The dynamics of histotripsy bubbles. In: Proceedings of the 10th international symposium for therapeutic ultrasound. Laurel, MD: International Society for Therapeutic Ultrasound; 2011. p. 427–430.

Lafon C, Zderic V, Noble M, Yuen J, Kaczkowski P, Sapozhnikov O, Chavrier F, Crum L, Vaezy S. Gel phantom for use in high-intensity focused ultrasound dosimetry. Ultrasound Med Biol 2005;31:1383–1389.

Lake AM, Hall TL, Kieran K, Fowlkes JB, Cain CA, Roberts WW. Histotripsy: Minimally invasive technology for prostatic tissue ablation in an *in vivo* canine model. Urology 2008;72:682–686.

Lin KW, Kim Y, Maxwell A, Wang TY, Hall TL, Xu Z, Fowlkes JB, Cain CA. Histotripsy beyond the intrinsic cavitation threshold using very short ultrasound pulses: Microtripsy. IEEE Trans Ultrason Ferroelectr Freq Control 2014;61:251–265.

Maxwell A, Sapozhnikov O, Bailey M, Crum L, Xu Z, Fowlkes B, Cain C, Khokhlova V. Disintegration of tissue using high intensity focused ultrasound: Two approaches that utilize shock waves. Acoust Today 2012;8:24–37.

Maxwell AD, Cain CA, Hall TL, Fowlkes JB, Xu Z. Probability of cavitation for single ultrasound pulses applied to tissues and tissue-mimicking materials. Ultrasound Med Biol 2013;39:449–465.

Maxwell AD, Wang TY, Cain CA, Fowlkes JB, Sapozhnikov OA, Bailey MR, Xu Z. Cavitation clouds created by shock scattering from bubbles during histotripsy. J Acoust Soc Am 2011;130:1888–1898.

Pahk KJ, Dhar DK, Malago M, Saffari N. Ultrasonic histotripsy for tissue therapy. J Phys Conf Ser 2015;581:012001.

Pahk KJ, Mohammad GH, Malago M, Saffari N, Dhar DK. A novel approach to ultrasound-mediated tissue decellularization and intrahepatic cell delivery in rats. Ultrasound Med Biol 2016;42:1958–1967.

Parsons JE, Cain CA, Abrams GD, Fowlkes JB. Pulsed cavitational ultrasound therapy for controlled tissue homogenization. Ultrasound Med Biol 2006;32:115–129.

Pennes HH. Analysis of tissue and arterial blood temperatures in the resting human forearm. J Appl Physiol 1948;1:93–122.

Pierce AD. Acoustics: An introduction to its physical principles and applications. New York: McGraw-Hill; 1989.

Pishchalnikov YA, Sapozhnikov OA, Bailey MR, Williams JC, Cleveland RO, Colonius T, Crum LA, Evan AP, McAteer JA. Cavitation bubble cluster activity in the breakage of kidney stones by lithotripter shockwaves. J Endourol 2003;17:435–446.

Roberts WW, Hall TL, Ives K, Wolf JS, Fowlkes JB, Cain CA. Pulsed cavitational ultrasound: A noninvasive technology for controlled tissue ablation (histotripsy) in the rabbit kidney. J Urol 2006;175:734–738.

Schade GR, Hall TL, Roberts WW. Urethral-sparing histotripsy of the prostate in a canine model. Urology 2012a;80:730–735.

Schade GR, Keller J, Ives K, Cheng X, Rosol TJ, Keller E, Roberts WW. Histotripsy focal ablation of implanted prostate tumor in an ACE-1 canine cancer model. J Urol 2012b;188:1957–1964.

Schade GR, Maxwell AD, Khokhlova T, Wang YN, Sapoznikov O, Bailey MR, Khokhlova V. Boiling histotripsy of the kidney: Preliminary studies and predictors of treatment effectiveness. J Acoust Soc Am 2014;136:2251.

Simon JC, Sapozhnikov OA, Khokhlova VA, Wang YN, Crum LA, Bailey MR. Ultrasonic atomization of tissue and its role in tissue fractionation by high intensity focused ultrasound. Phys Med Biol 2012; 57:8061–8078.

Simon JC, Sapozhnikov OA, Wang YN, Khokhlova VA, Crum LA, Bailey MR. Investigation into the mechanisms of tissue atomization by high-intensity focused ultrasound. Ultrasound Med Biol 2015;41:1372–1385.

Soneson JE. A user-friendly software package for HIFU simulation. In: Proceedings of the 8th international symposium for therapeutic ultrasound. Laurel, MD: International Society for Therapeutic Ultrasound; 2009. p. 165–169.

Styn NR, Wheat JC, Hall TL, Roberts WW. Histotripsy of vx-2 tumor implanted in a renal rabbit model. J Endourol 2010;24:1145–1150.

Tavakkoli J, Birer A, Arefiev A, Prat F, Chapelon JY, Cathignol D. A piezocomposite shock wave generator with electronic focusing capability: Application for producing cavitation-induced lesions in rabbit liver. Ultrasound Med Biol 1997;23:107–115.

ter Haar G, Coussios C. High intensity focused ultrasound: Physical principles and devices. Int J Hyperthermia 2007;23:89–104.

Vlaisavljevich E, Kim Y, Allen S, Owens G, Pelletier S, Cain C, Ives K, Xu Z. Image-guided non-invasive ultrasound liver ablation using histotripsy: Feasibility study in an *in vivo* porcine model. Ultrasound Med Biol 2013;39:1398–1409.

Vlaisavljevich E, Lin KW, Maxwell A, Warnez MT, Mancia L, Singh R, Putnam AJ, Fowlkes B, Johnsen E, Cain C, Xu Z. Effects of ultrasound frequency and tissue stiffness on the histotripsy intrinsic threshold for cavitation. Ultrasound Med Biol 2015a;41:1651–1667.

Vlaisavljevich E, Lin KW, Warnez MT, Singh R, Mancia L, Putnam AJ, Johnsen E, Cain C, Xu Z. Effects of tissue stiffness, ultrasound frequency, and pressure on histotripsy-induced cavitation bubble behavior. Phys Med Biol 2015b;60:2271–2292.

Vlaisavljevich E, Maxwell A, Warnez M, Johnsen E, Cain CA, Xu Z. Histotripsy-induced cavitation cloud initiation thresholds in tissues of different mechanical properties. IEEE Trans Ultrason Ferroelectr Freq Control 2014;61:341–352.

Vlaisavljevich E, Xu Z, Maxwell AD, Mancia L, Zhang X, Lin KW, Duryea AP, Sukovich JR, Hall TL, Johnsen E, Cain CA. Effects of temperature on the histotripsy intrinsic threshold for cavitation. IEEE Trans Ultrason Ferroelectr Freq Control 2016;63:1064–1077.

Wang YN, Khokhlova T, Bailey M, Hwang JH, Khokhlova V. Histological and biochemical analysis of mechanical and thermal bioeffects in boiling histotripsy lesions induced by high intensity focused ultrasound. Ultrasound Med Biol 2013;39:424–438.

Xu Z, Owens G, Gordon D, Cain C, Ludomirsky A. Noninvasive creation of an atrial septal defect by histotripsy in a canine model. Circulation 2010;121:742–749.

Zhou Y, Gao XW. Variations of bubble cavitation and temperature elevation during lesion formation by high-intensity focused ultrasound. J Acoust Soc Am 2013;134:1683–1694.

Zhu S, Cocks FH, Preminger GM, Zhong P. The role of stress waves and cavitation in stone comminution in shock wave lithotripsy. Ultrasound Med Biol 2002;28:661–671.